Oceanologia (2016) 58, 59—70

Available online at www.sciencedirect.com

ScienceDirect

journal homepage: www.elsevier.com/locate/oceano

ORIGINAL RESEARCH ARTICLE

On the nonlinear internal waves propagating in an inhomogeneous shallow sea

Stanisław R. Massel *

Institute of Oceanology of the Polish Academy of Sciences, Sopot, Poland

Received 6 November 2015; accepted 22 January 2016
Available online 16 February 2016

KEYWORDS
Internal waves;
Energy flux conservation;
Bottom friction;
Shearing instability;
Wave breaking

Summary A concept of conservation of energy flux for the internal waves propagating in an inhomogeneous shallow water is examined. The emphasis is put on an application of solution of the Korteweg—de Vries (KdV) equation in a prescribed form of the cnoidal and solitary waves. Numerical simulations were applied for the southern Baltic Sea, along a transect from the Bornholm Basin, through the Słupsk Sill and Słupsk Furrow to the Gdańsk Basin. Three-layer density structure typical for the Baltic Sea has been considered. An increase of wave height and decrease of phase speed with shallowing water depth was clearly demonstrated. The internal wave dynamics on both sides of the Słupsk Sill was found to be different due to different vertical density stratification in these areas. The bottom friction has only negligible influence on dynamics of internal waves, while shearing instability may be important only for very high waves. Area of possible instability, expressed in terms of the Richardson number *Ri*, is very small, and located within the non-uniform density layer, close to the interface with upper uniform layer. Kinematic breaking criteria have been examined and critical internal wave heights have been determined.

1. Introduction

A sea bottom is only seldom horizontal and usually water depth and vertical density structure are varying in space and time. Observations of internal waves in the Andaman Sea, Sulu Sea, Australian North West Shelf and the South China Sea, as well as in other sea basins, show that shoaling effects and local bottom changes may influence essentially the

* Correspondence to: Institute of Oceanology of the Polish Academy of Sciences, 81-712 Sopot, Poland. Tel.: +48 587311815.
E-mail address: smas@iopan.gda.pl.
Peer review under the responsibility of Institute of Oceanology of the Polish Academy of Sciences.

Production and hosting by Elsevier

http://dx.doi.org/10.1016/j.oceano.2016.01.005

internal wave evolution. At present, the South China Sea is known as a "hot spot" for observations of the internal waves generated by tides in deep sea and propagating on the ocean shelf (Lien et al., 2014). A large-amplitude depression of the first mode of the internal solitary waves has been observed during spring tide using both shipboard and mooring ADCP and CTD measurements. Maximum negative vertical displacement approached the value of 100–150 m, nearly half of the water depth, and observed phase velocity was equal to about 2 m s^{-1}. Comprehensive observations of the internal tides by Holloway (1994, 1996) in a region of shelf-break on the Australian North West Shelf showed that internal tides exhibit a three-dimensional structure. Waves of depression are observed during summer, while in winter they are weaker and are waves of positive elevation.

Satellite SAR images provided an excellent tool for observation and recording of the internal waves in the ocean. The Indonesian Throughflow, the Middle Atlantic Bight, the Gulf of Aden and the White Sea are only a few examples of such locations. Other examples have been collected and discussed by Massel (2015).

Except the observations in nature, several attempts of modelling of the internal waves have been reported. Vlasenko and Hutter (2002) using numerical simulations, studied transformation of large amplitude internal solitary waves over a slope-shelf topography. Grimshaw et al. (2004) employed the extended Korteweg-de Vries (eKdV) equation to simulate propagation of internal solitary waves taking into account a real variability of wave parameters for several oceanic shelves. It was shown that if the background environment varies sufficiently slowly in comparison with an individual solitary wave, then the wave has a soliton-like form with varying amplitude and phase for large distances.

Combined effect of the Earth rotation and varying bathymetry on the solitary internal waves propagating on long distances was described by Grimshaw et al. (2014) using an extension of the KdV equation in the form of the Ostrovsky equation. The main finding of this study is that the Earth rotation induces a formation of a secondary wave packet, trailing behind the leading wave. These results correspond to bottom topography and density stratification for the cross section on the South China Sea. However, as the authors argued, they are rather typical for many other continental slopes.

In contrast to the deep sea there are not numerous papers on the internal waves dynamics in the shallow water. The application of the concept of conservation of energy flux to study the long internal wave dynamics in the horizontally inhomogeneous ocean was reported by Pelinovsky and Shavratsky (1976) and Pelinovsky et al. (1994), however without any connections to the real bathymetry and density stratification. Laboratory experiments and theoretical studies have been conducted by Helfrich and Melville (1986) and Helfrich (1992) to explore shoaling of the internal solitary waves of depression in a two-layer system on a uniform slope. An extended Korteweg-de Vries (eKdV) equation, including the nonlinearity, dispersion and dissipation was solved numerically for single and rank-ordered pairs of solitary waves incident on the slope-shelf topography of large dimension when the topographic effects dominate nonlinearity and dispersion. The authors discussed an application of the developed theoretical models for the real oceanographic situations, however expressing some doubts to which extent a laminar damping in the laboratory tanks properly reflects turbulent eddy viscosity in the real ocean.

In this paper, numerical simulations of long internal waves motion over a slowly changing bathymetry and density stratification in the southern Baltic Sea are considered. For analysis, the typical temperature and salinity vertical structure, recorded during the cruise of the research vessel s/v *Oceania* in February 2003 along the transect from Bornholm Basin, through Słupsk Sill and Słupsk Furrow to Gdańsk Basins (see Fig. 1) was used. This period corresponded to one of the major inflows of saline water from the North Sea to the Baltic Sea and high dynamics of the pycnocline motions (Massel, 2015; Piechura and Beszczyńska-Möller, 2004).

A concept of the energy flux conservation was considered under the assumption that the internal wave maintains its cnoidal-like shape with varying wave parameters. Also, the limiting cases of the cnoidal wave, namely the solitary and sinusoidal waves are taken into account. In the numerical simulations, the non-dissipative motion, as well as motion with several dissipative mechanisms, such as bottom friction, shearing instability with mixing and wave breaking, have been taken into account.

The paper is organised as follows. In Section 2, the concept of energy flux conservation for internal waves is introduced. In Section 3, motion of the internal waves of prescribed form is discussed and governing equations are solved. Finally, variation of the wave height and wave shape are determined and illustrated for given locations along the transect in the southern Baltic Sea. The major conclusions are formulated in Section 4.

2. Concept of the energy flux conservation

We would like to consider a long internal wave motion in two-dimensional vertical plane (x, z) with z-axis positive upward. Water depth is slowly varying in the x direction and the refraction effects are omitted. The background density $\overline{\rho}(x,z)$ is a known slowly varying function of x and z coordinates. Under the Boussinesq approximation, the rate of wave energy change can be presented as follows (Kundu et al., 2016; Massel, 2015):

$$\frac{\partial}{\partial t}\left[\frac{1}{2}\overline{\rho}(x,z)(u^2+w^2)\right]+g\rho(z)w+\nabla\cdot(pu)=0, \tag{1}$$

where u and w are the velocity components in x and z direction, respectively, p is the water pressure and $\rho(z)$ is the perturbation of density component due to wave action. The first term in Eq. (1) represents a rate of change of the kinetic energy and the second term can be considered as the rate of change of potential energy. The last term is the net work done by the pressure forces and it can be interpreted as the divergence of the energy flux pu (Gill, 1982).

Therefore, the energy flux integrated over water depth and averaged over wave period can be written as follows:

$$\overline{F_E(x)}=\frac{1}{T}\int_0^T\int_{-h(x)}^0 p(x,z,t)u(x,z,t)\,dz\,dt, \tag{2}$$

in which $T=2\pi/\omega$ is the internal wave period and ω is the wave frequency.

To determine the energy flux $\overline{F_E(x)}$ we consider the vertical displacements of isopycnals due to long internal

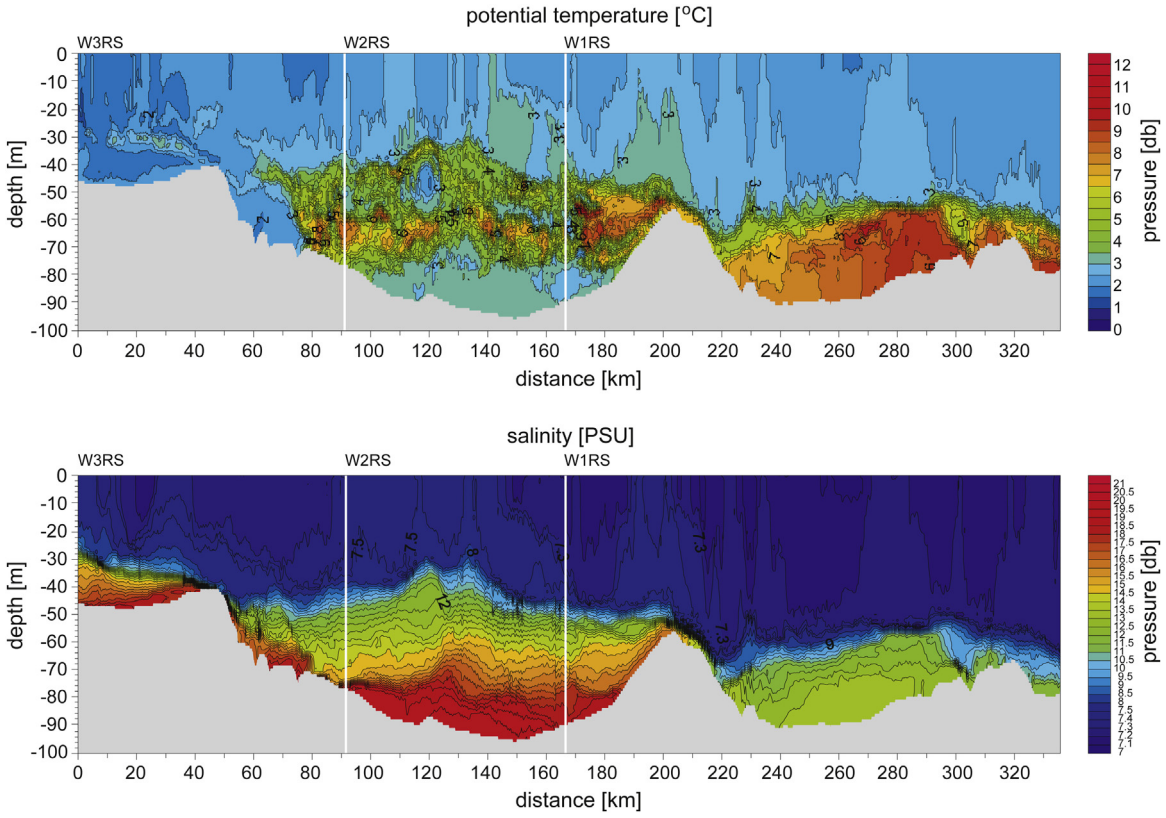

Figure 1 Water depths, water temperature and salinity in the Bornholm Basin, Słupsk Sill and Słupsk Furrow on February 4—6, 2003 (Piechura and Beszczyńska-Möller, 2004).

waves in the form (Grimshaw et al., 2004; Kurkina et al., 2011; Massel, 2015):

$$\zeta(x,z,t) = \eta(x,t)\Phi(x,z), \tag{3}$$

in which $\eta(x, t)$ describes an evolution of the internal wave shape in space and time, and function $\Phi(x, z)$ determines a vertical modal structure of the internal wave.

Among a variety of approaches to describe an evolution of the long periodic internal waves, the Korteweg-de Vries (KdV) theory (Korteweg and de Vries, 1895; Massel, 1989; Miles, 1981; Whitham, 1974) is applied where the balance between nonlinearity and dispersion of wave motion is included:

$$\frac{\partial\eta}{\partial t} + C_p\frac{\partial\eta}{\partial x} + \alpha\eta\frac{\partial\eta}{\partial x} + \beta\frac{\partial^3\eta}{\partial x^3} = 0, \tag{4}$$

in which C_p is the linear phase velocity, α is the nonlinearity parameter and β is the dispersion parameter.

The function $\Phi(x, z)$ in Eq. (3) is a solution of the eigenvalue problem which in the Boussinesq approximation becomes (Massel, 2015):

$$\frac{d^2\Phi(x,z)}{dz^2} + \frac{N^2(x,z)-\omega^2}{\omega^2-f^2}k^2(x)\Phi(x,z) = 0, \tag{5}$$

where $k(x)$ is the horizontal wavenumber, f is the inertial frequency and $N(x, z)$ is the Väisälä-Brunt frequency:

$$N^2(x,z) = -\frac{g}{\overline{\rho}(x,z)}\frac{d\overline{\rho}(x,z)}{dz}, \tag{6}$$

in which $\overline{\rho}(x,z)$ is the background density.

Function $\Phi(x, z)$ is defined for the water column ($-h \le z \le 0$) and the boundary conditions are:

$$\Phi(x,0) = \Phi(x,-h) = 0. \tag{7}$$

The above boundary value problem should be valid for each mode, n, and the wave frequency ω should be bounded above by the Väisälä-Brunt frequency, $N(x, z)$, and below by the inertial frequency, f, i.e.:

$$f^2 < \omega^2 < N^2(x,z). \tag{8}$$

For long periodic waves if $\omega^2 \ll N^2(x, z)$ and when the Earth rotation is neglected, we obtain:

$$N^2(x,z)-\omega^2 \approx N^2(x,z), \quad \omega^2-f^2 \approx \omega^2. \tag{9}$$

Thus, Eq. (5) for function $\Phi(x, z)$ can be rewritten as follows:

$$\frac{d^2\Phi(x,z)}{dz^2} + q(x,z)\lambda\Phi(x,z) = 0, \tag{10}$$

where

$$q(x,z) = N^2(x,z), \qquad \lambda = \frac{1}{C_p^2(x)}. \tag{11}$$

The solution of Eq. (10) is described fully in Section 3.2.3 for an inhomogeneous three-layer density stratification. Here we only note that the function $\Phi(x, z)$ is normalised so that maximum value of the function $\Phi(x, z)$ is equal to 1 at some level z, and $\Phi(x, z)$ vanishes at the sea surface and sea bottom. For a given frequency ω, solution of Eq. (10) shows

that an initial disturbance is decomposed into a set of propagating modes λ_n with corresponding phase velocities $C_p^{(n)}$. However for further analysis, the first most energetic mode (eigenvalue) $\lambda = \lambda_1$ is retained, with the phase velocity given by Eq. (11). It should be noted here that phase velocity $C_p(x)$ is totally dependent on the vertical water stratification and Väisälä-Brunt frequency, and it does not depend on the internal wave amplitude.

From the following expressions for the dynamic pressure p and horizontal velocity u (Krauss, 1966; Kurkina et al., 2011; Kundu et al., 2016):

$$p(x,z) = -\overline{\rho}(x,z)C_p(x)u(x,z) \quad \text{and} \quad u(x,z) = -C_p(x)\eta(x,t)\frac{d\Phi(x,z)}{dz}, \tag{12}$$

the energy flux integrated over water depth and averaged over wave period becomes:

$$\overline{F_E(x)} = \frac{1}{T}\int_0^T\int_{-h(x)}^0 C_p^3(x)\overline{\rho}(x,z)\eta^2(x,t)\left(\frac{d\Phi(x,z)}{dz}\right)^2 dz\,dt, \tag{13}$$

or:

$$\overline{F_E(x)} = C_p^3(x)\Pi(x)\frac{1}{T}\int_0^T \eta^2(x,t)\,dt, \tag{14}$$

where

$$\Pi(x) = \int_{-h(x)}^0 \overline{\rho}(x,z)\left(\frac{d\Phi(x,z)}{dz}\right)^2 dz. \tag{15}$$

Functions $C_p(x)$ and $\Pi(x)$ depend totally on the vertical stratification of water masses at a given distance x and they do not depend on time.

Now we assume the conservation of energy flux for a given dissipation mechanisms in the general form:

$$\frac{\partial\overline{F_E(x)}}{\partial x} + D(x) = 0, \tag{16}$$

in which $D(x)$ is the dissipation term. This term obeys the possible energy losses due to bottom friction, percolation within the sea bottom, shearing instability and mixing in water column, and wave breaking.

3. Propagation of long internal waves on slowly varying water depth

3.1. Governing equations

In general, the energy flux conservation concept should be valid for arbitrary internal wave shape $\eta(x, t)$. However, determination of initial $\eta(x_0, t)$ function is very difficult to achieve in the natural conditions. Therefore we will consider an evolution of long internal waves with isopycnal displacements given in a prescribed form of the periodic cnoidal waves. The cnoidal waves resulting from the KdV equation were chosen as they provide an opportunity to study dynamics of the simple linear sinusoidal waves as well as solitary waves within the same framework of the Jacobian elliptic functions (Abramowitz and Stegun, 1975).

Thus we assume the wave shape as follows (Massel, 1989, 2015):

$$\eta(x,t) = H(x)\left\{\frac{1}{m}\left(1-\frac{\mathbf{E}}{\mathbf{K}}-m\right) + cn^2\left[\frac{2\mathbf{K}}{L}(x-Ut)\right]\right\}, \tag{17}$$

in which $H(x)$ is the wave height, L is the wave length, $cn(x)$ is the Jacobian elliptic function, and $\mathbf{K}$ and $\mathbf{E}$ are the complete elliptic integrals of the first and second kind, respectively. They are functions of the elliptic parameter m from the range $0 \le m \le 1$ (Abramowitz and Stegun, 1975). The phase speed U is given by:

$$U = C_p(x)\left[1 + \frac{\hat{\alpha}H(x)}{3m}\left(2-3\frac{\mathbf{E}}{\mathbf{K}}-m\right)\right]. \tag{18}$$

The wave height $H(x)$ corresponds to the maximum isopycnal displacement ζ at a level z where the normalised function $\Phi(x, z) = 1$. Due to boundary conditions (7), the isopycnal displacements at sea surface and sea bottom are equal to zero.

To define an unknown elliptic parameter m, the following relationship is applied (Massel, 1989, 2015):

$$\left(\frac{\hat{\alpha}}{\hat{\beta}}\right)\frac{H(x)L^2}{48} = m\mathbf{K}^2, \tag{19}$$

or

$$\left(\frac{\hat{\alpha}(x)}{\hat{\beta}(x)}\right)\frac{H(x)(C_p(x)\,T)^2}{48} = \frac{m\mathbf{K}^2}{\left[1+\frac{\hat{\alpha}(x)H(x)}{3m}\left(2-3\frac{\mathbf{E}}{\mathbf{K}}-m\right)\right]^2}, \tag{20}$$

in which nonlinearity and dispersion parameters $\hat{\alpha}$ and $\hat{\beta}$ are:

$$\hat{\alpha}(x) = \frac{\alpha(x)}{C_p(x)} = \frac{3}{2}\frac{\int_{-h(x)}^0\left(\frac{d\Phi(x,z)}{dz}\right)^3 dz}{\int_{-h(x)}^0\left(\frac{d\Phi(x,z)}{dz}\right)^2 dz}, \tag{21}$$

$$\hat{\beta}(x) = \frac{\beta}{C_p(x)} = \frac{1}{2}\frac{\int_{-h(x)}^0\Phi^2(x,z)\,dz}{\int_{-h(x)}^0\left(\frac{d\Phi(x,z)}{dz}\right)^2 dz}. \tag{22}$$

To get the energy flux we have to solve the integral in Eq. (14) for $\eta(x, t)$ given by Eq. (17). The calculations are facilitated by a recursion relations from Gradshteyn and Ryzhik (1965):

$$I(l) = \frac{1}{\mathbf{K}}\int_0^K [m\,cn^2(\theta)]^l d\theta; \tag{23}$$

then:

$$I(0) = 1 \quad \text{and} \quad I(1) = -1 + m + \frac{\mathbf{E}}{\mathbf{K}}, \tag{24}$$

and:

$$I(l+2) = \left(\frac{2l+2}{2l+3}\right)(2m-1)I(l+1) + \left(\frac{2l+1}{2l+3}\right) \times (m-m^2)I(l). \tag{25}$$

Using these relationships an evolution equation for wave height becomes:

$$\frac{\partial}{\partial x}\left(C_p^3(x)\Pi(x)\sum_{i=1}^{i=3}A_i(x)H^2(x)\right)+D(x)=0, \tag{26}$$

or

$$\frac{dH(x)}{dx}+\frac{1}{2}\frac{\frac{dP_1(x)}{dx}}{P_1(x)}H(x)+\frac{1}{2}\frac{D(x)}{P_1(x)H(x)}=0, \tag{27}$$

in which

$$P_1(x)=C_p^3(x)\Pi(x)\sum_{i=1}^{i=3}A_i(x), \tag{28}$$

$$A_1(x)=\left[\frac{1}{m}\left(1-\frac{\mathbf{E}}{\mathbf{K}}-m\right)\right]^2, \tag{29}$$

$$A_2(x)=-\frac{2}{m^2}\left(1-\frac{\mathbf{E}}{\mathbf{K}}-m\right)^2, \tag{30}$$

$$A_3(x)=\frac{1}{3m^2}\left[2(1-2m)\left(1-m-\frac{\mathbf{E}}{\mathbf{K}}\right)+m(1-m)\right]. \tag{31}$$

Prior to solving Eq. (27), the dissipation term $D(x)$ should be determined. In the following reasoning, various dissipation mechanisms are discussed. However, it will be useful to start with case of the non-dissipative motion.

3.2. Wave motion without energy dissipation

When dissipation is totally neglected, i.e. $D(x) = 0$, solution of Eq. (27) takes the form:

$$H(x)=\left(\frac{C_p(x_0)}{C_p(x)}\right)^{3/2}\left(\frac{\Pi(x_0)}{\Pi(x)}\right)^{1/2}\left[\frac{\sum_{i=1}^{i=3}A_i(x_0)}{\sum_{i=1}^{i=3}A_i(x)}\right]^{1/2}H(x_0), \tag{32}$$

where x_0 denotes the reference point where the values $C_p(x_0)$, $\Pi(x_0)$ and $A_i(x_0)$ are assumed to be known.

3.2.1. Solitary wave

The above formula for the cnoidal waves is simplified considerably for extreme values of the elliptic parameter m, namely for $m = 1$ and $m = 0$. When $m \to 1$, we have $\mathbf{E} = 1$ and $\mathbf{K} \to \infty$. Consequently $L \to \infty$, and function $cn^2(u) \to \cosh^{-2}(u)$. Thus the solitary wave shape becomes:

$$\eta(x,t)=H(x)\cosh^{-2}\left[\left(\frac{H(x)}{12}\frac{\hat{\alpha}(x)}{\hat{\beta}(x)}\right)^{1/2}(x-Ut)\right], \tag{33}$$

where

$$U=C_p(x)\left(1+\frac{1}{3}\hat{\alpha}(x)H(x)\right)\approx C_p(x). \tag{34}$$

For averaged energy flux for the solitary waves we have:

$$\overline{F_E(x)}=\frac{4}{\sqrt{3}}C_p^2(x)\Pi(x)\left(\frac{\beta(x)}{\alpha(x)}\right)^{1/2}H^{3/2}. \tag{35}$$

Thus, if $D(x) = 0$ from Eq. (27) we find:

$$H(x)=E_1(x)\,E_2(x)\,E_3(x)\,H(x_0), \tag{36}$$

where:

$$\left.\begin{aligned}E_1(x)&=\left(\frac{C_p(x)(x_0)}{C_p(x)(x)}\right)^{4/3}\\ E_2(x)&=\left[\left(\frac{\hat{\alpha}(x)}{\hat{\alpha}(x_0)}\right)\left(\frac{\hat{\beta}(x_0)}{\hat{\beta}(x)}\right)\right]^{1/3}\\ E_3(x)&=\left(\frac{\Pi(x_0)}{\Pi(x)}\right)^{2/3}\end{aligned}\right\}. \tag{37}$$

Let us rewrite Eq. (36) as follows:

$$H(x)=C_p^{-4/3}(x)\,\Pi^{-2/3}(x)q^{1/3}(x)\,D_{\mathrm{ref}}, \tag{38}$$

in which:

$$q(x)=\frac{\int_{-h}^{0}\left(\frac{d\Phi(x,z)}{dz}\right)^3dz}{\int_{-h}^{0}\Phi^2(x,z)\,dz}, \tag{39}$$

and

$$D_{\mathrm{ref}}=C_p^{4/3}(x_0)\,\Pi^{2/3}(x_0)q^{-1/3}(x_0)H(x_0). \tag{40}$$

Expression (40) is in full agreement with results of Pelinovsky and Shavratsky (1976) obtained by another methods.

In a similar way we can determine the amplitudes of velocities and water density, i.e.:

$$\left.\begin{aligned}&\text{vertical velocity}\approx C_p^{-4/3}(x)\Pi^{-2/3}(x)q^{1/3}(x)\\ &\text{horizontal velocity}\approx C_p^{-1/3}(x)\Pi^{-2/3}(x)q^{1/3}(x)\frac{d\Phi(x,z)}{dz}\\ &\text{water density}\approx C_p^{-4/3}(x)\Pi^{-2/3}(x)q^{1/3}(x)\Phi(x,z)\frac{d\overline{\rho}(x,z)}{dz}\end{aligned}\right\}. \tag{41}$$

3.2.2. Linear wave

In the second extreme case when the parameter $m \to 0$, the complete elliptic integrals $\mathbf{E} = \mathbf{K} = \pi/2$. Therefore the first term in Eq. (17) becomes:

$$\lim\left[\frac{1}{m}\left(1-\frac{\mathbf{E}}{\mathbf{K}}-m\right)\right]=-1/2, \tag{42}$$

and

$$cn^2\left[\frac{2\mathbf{K}}{L}Ut\right]\to\cos^2\left[\frac{\pi}{L}C_p(x)t\right]. \tag{43}$$

Now the wave shape becomes:

$$\begin{aligned}\eta(x,t)&=-\frac{H(x)}{2}+H(x)\cos^2\left[\frac{\pi}{L}C_p(x)t\right]\\ &=\frac{H(x)}{2}\cos\left[\frac{2\pi}{L}C_p(x)t\right],\end{aligned} \tag{44}$$

and for wave height $H(x)$ we have:

$$H(x)=\left(\frac{C_p(x)(x_0)}{C_p(x)(x)}\right)^{3/2}\left(\frac{\Pi(x_0)}{\Pi(x)}\right)^{1/2}H(x_0). \tag{45}$$

3.2.3. Numerical simulation for an inhomogeneous three-layer water density structure

To illustrate the applicability of above formulae we assume for a moment that the dissipation energy is absent and the

internal waves are propagating over slowly changing water depth in the southern Baltic Sea. Two sections of the sloping bottom in region of the Słupsk Sill and the Słupsk Furrow have been chosen for numerical simulation. The first section of length of about 27 km extends from Stations 172 till Station 199. Numbers of Stations correspond to the distances given in Fig. 1. Water depth is changing from about 90 m in the Bornholm Basin to about 55 m close to the Słupsk Sill. Thus, the mean bottom slope is ~0.0011. The experimental data on the density stratification $\overline{\rho}(x,z)$ were obtained from the s/v *Oceania* cruises in February 2003. They confirm that the three-layer vertical density distribution dominates in the Baltic Sea (Krauss, 1966; Massel, 2015). The upper and bottom layers are usually uniform and the non-uniform layer between them is characterised by slowly changing density as follows:

$$\overline{\rho}(z)=\begin{cases}\rho_1 & \text{for } -h_1\le z\le 0\\ \rho_1\exp\left[-\dfrac{N_0^2(x)}{g}(z+h_1)\right] & \text{for } -h_2\le z\le -h_1\\ \rho_2 & \text{for } -h\le z\le -h_2\end{cases}, \tag{46}$$

in which h is total water depth, h_1 is the thickness of upper layer, (h_2-h_1) is the thickness of the non-uniform layer, $(h-h_2)$ is the thickness of bottom uniform layer and $N_0(x)$ is the Väisälä-Brunt frequency given as:

$$N_0^2(x)=\begin{cases}0 & \text{for } -h_1\le z\le 0\\ \dfrac{g\ln\left(\frac{\varrho_1}{\varrho_2}\right)}{h_1-h_2} & \text{for } -h_2\le z\le -h_1\\ 0 & \text{for } -h\le z\le -h_2\end{cases} \tag{47}$$

Solution of the linear eigenvalue problem (see Eq. (10)) for long internal waves with a given density distribution can be obtained by an analytical method. In particular, we adopt the function $\Phi(x,z)$ in the form:

$$\Phi(x,z)=\begin{cases}B(x)z & -h_1\le z\le 0\\ C(x)\cos(\gamma z)+D(x)\sin(\gamma z) & -h_2\le z\le -h_1\\ E(x)(z+h) & -h\le z\le -h_2\end{cases} \tag{48}$$

where $\gamma=N_0(x)/C_p(x)$.

The functions $B(x)$, $C(x)$, $D(x)$ and $E(x)$ are obtained from the continuity conditions at the sublayers boundaries. These conditions are expressed in the form of continuity of function $\Phi(x,z)$ and its gradient $d\Phi(x,z)/dz$ across the boundaries (Massel, 2015). The resulted set of equations has a non-trivial solution only when the following determinant Δ becomes zero:

$$\Delta=\begin{vmatrix}a_{11} & a_{12} & a_{13} & a_{14}\\ a_{21} & a_{22} & a_{23} & a_{24}\\ a_{31} & a_{32} & a_{33} & a_{34}\\ a_{41} & a_{42} & a_{43} & a_{44}\end{vmatrix}=0, \tag{49}$$

in which:

$$\left.\begin{array}{llll}a_{11}=h_1, & a_{12}=\cos(\gamma h_1), & a_{13}=-\sin(\gamma h_1), & a_{14}=0\\ a_{21}=1, & a_{22}=-\gamma\sin(\gamma h_1), & a_{23}=-\gamma\cos(\gamma h_1), & a_{24}=0\\ a_{31}=0, & a_{32}=-\cos(\gamma h_2), & a_{33}=\sin(\gamma h_2), & a_{34}=h-h_2\\ a_{41}=0, & a_{42}=-\gamma\sin(\gamma h_2), & a_{43}=-\gamma\cos(\gamma h_2), & a_{44}=1\end{array}\right\}. \tag{50}$$

For a given value of the Väisälä-Brunt frequency $N_0(x)$, Eq. (49) allows to determine the phase velocities $C_p(x)$ for an infinite number of modes, n, and corresponding functions for a given mode are:

$$\left.\begin{aligned}C(x)&=\frac{a_{13}a_{21}-a_{11}a_{23}}{a_{12}a_{23}-a_{13}a_{22}}B(x)\\ D(x)&=\frac{a_{11}a_{22}-a_{12}a_{21}}{a_{12}a_{23}-a_{13}a_{22}}B(x)\\ E(x)&=\frac{-(a_{32}C(x)+a_{33}D(x))}{a_{34}}\end{aligned}\right\}. \tag{51}$$

Now we apply above formulae for the first mode of the internal solitary wave moving over the west slope of the Słupsk Sill. The scattered rhombuses in Fig. 2 show the solitary wave height increase with a distance x, when approaching to the Słupsk Sill, what should be expected. Spreading of dots results from the variation in space of the experimental temperature and salinity values which are initial ones for determination of density stratification according to UNESCO formula (Massel, 2015). Solid line represent the best fitting of the simulation data. These remarks also apply for other figures in the paper.

It should be noted that on the distance of about 30 km, the non-dimensional wave height has increased more than two times with respect to wave height at the reference point. In the same time, the circular dots demonstrate a slower decrease of the non-dimensional phase velocity $C_p(x)$.

Fig. 3 illustrates an important dependence of the solitary non-dimensional wave height and phase velocity on water depth. Non-dimensional wave height is decreasing approximately as the function $H(x)/H(x_0)\approx h^{-2.67}$ while the phase velocity increase is approximated by the linear function of $C_p(x)/C_p(x_0)\approx 0.015h-0.21$. In Fig. 4 the known fact that the dispersion parameter β depends mostly on the water depth h is confirmed. For both regions under consideration, parameter β is almost a linear function of water depth. However values of parameter β for the same water depths are different for both slopes what suggests that the dispersion parameter β possibly depends also on another factors. For deeper waters in the Gotland Deep in the Baltic Sea,

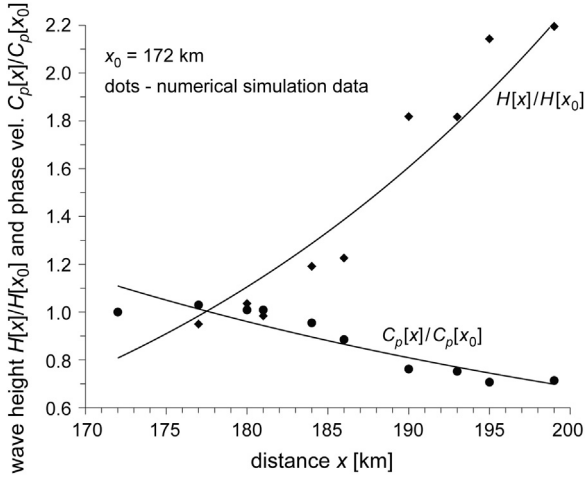

Figure 2 Non-dimensional wave height and phase velocity as a function of distance for the west slope of the Słupsk Sill. Solid curves denote the best fitting of simulation data.

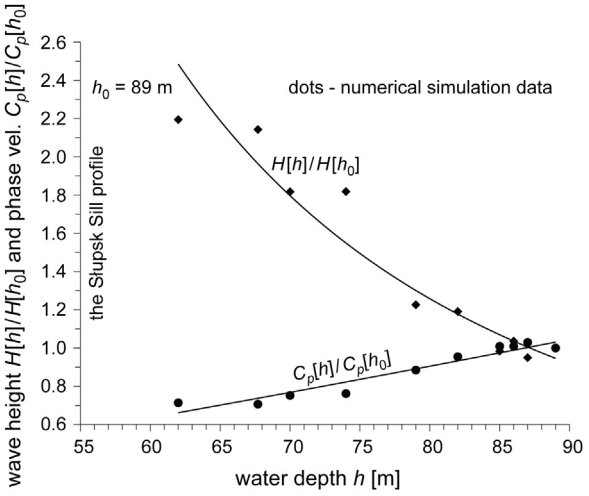

Figure 3 Non-dimensional wave height and phase velocity as a function of water depth for the west slope of the Słupsk Sill. Solid curves denote the best fitting of simulation data.

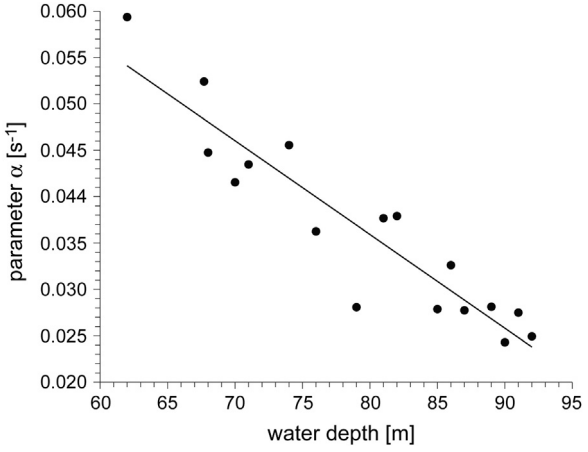

Figure 5 Nonlinear parameter α as a function of water depth. Solid curves denote the best fitting of simulation data.

Talipova et al. (1998) showed that $\beta = 2.12 \cdot 10^{-6} h^{3.86}$ and phase velocity $C_p = 0.82 \ln(h) - 3.4$.

As shown in Fig. 5, the nonlinear parameter α linearly attenuates with the water depth for both regions under consideration, i.e. $\alpha \approx -0.001h + 0.117$. It means that internal waves climbing on the west slope of the Słupsk Sill and on the east slope of the Słupsk Furrow become more and more nonlinear, what should be expected. Moreover, Fig. 6 shows a linear relationship between wave height H and the function $C_p^{-4/3}(x)$ (see Eq. (38). From this equation it follows that under assumption of constant energy flux, when water depth decreases, the solitary wave height increases and the crest of a solitary wave becomes higher and wave shape becomes thinner as shown in Fig. 7).

Similar numerical simulations have been performed for east slope of the Słupsk Furrow for Stations 244—318 (see Fig. 1). Comparison of the phase velocities given in Fig. 8 showed that $C_p(x)$ for this slope is smaller than phase velocity on west slope of the Słupsk Sill.

From Eq. (10) follows that except water depth, the phase velocity $C_p(x)$ depends on the Väisälä-Brunt frequency $N_0(x)$ which is a function of the vertical stratification of water density. So, let us write:

$$\frac{C_p(x)}{\sqrt{gh(x)}} = f\left(\frac{\rho_2 - \rho_1}{\rho_1 + \rho_2}\right), \tag{52}$$

where the ratio $(\rho_2 - \rho_1)/(\rho_1 + \rho_2)$ can be called as a density parameter. Function (52) is shown in Fig. 9 for both regions under consideration. The non-dimensional phase velocities form two separated groups depending on the density parameter. Larger value of this parameter yields the higher value of the phase velocity for the west slope of the Słupsk Sill than for the other region. However within each group of data, the non-dimensional phase velocity is almost linearly dependent on the density parameter:

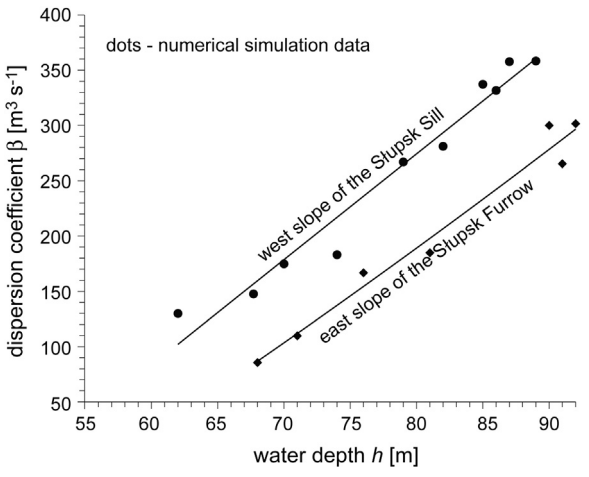

Figure 4 Dispersion parameter β as a function of water depth. Solid curve denotes the best fitting of simulation data.

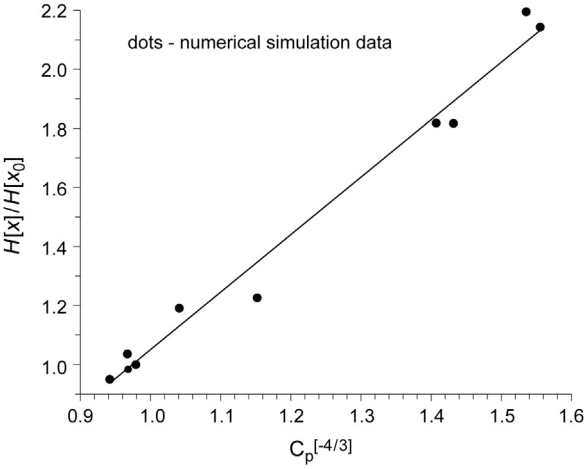

Figure 6 Non-dimensional wave height as a function of phase velocity for the west slope of the Słupsk Sill. Solid curve denotes the best fitting of simulation data.

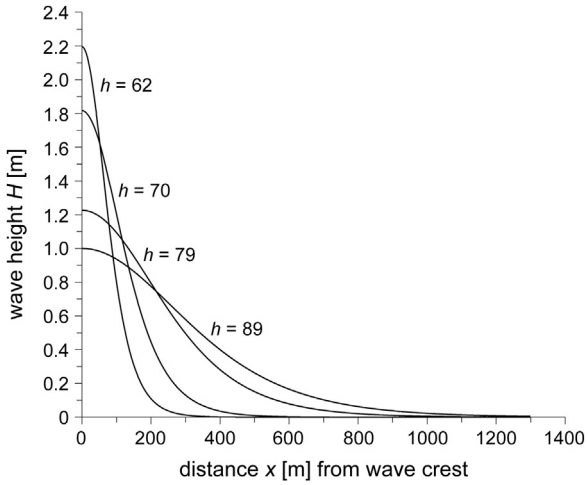

Figure 7 Internal wave shape as a function of distance from wave crest for chosen water depths.

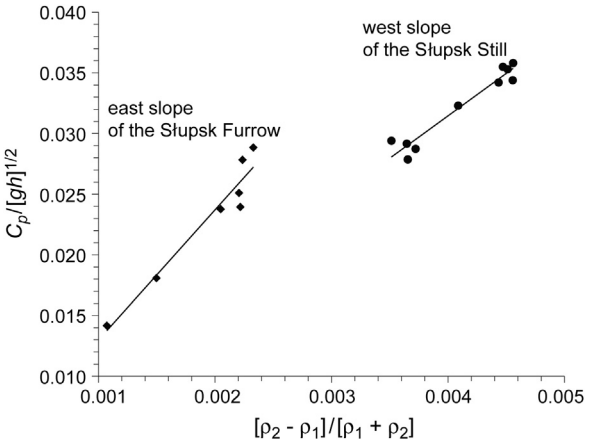

Figure 9 Non-dimensional phase velocity as a function of density parameter for the west slope of the Słupsk Sill and the east slope of the Słupsk Furrow. Solid curves denote the best fitting of simulation data.

$$\frac{C_p(x)}{\sqrt{gh(x)}} = \begin{cases} 7.0\left(\dfrac{\rho_2-\rho_1}{\rho_1+\rho_2}\right) & \text{for west slope of the Słupsk Sill} \\ 10.7\left(\dfrac{\rho_2-\rho_1}{\rho_1+\rho_2}\right) & \text{for east slope of the Słupsk Furrow} \end{cases} \tag{53}$$

From the above analysis it follows that the Słupsk Sill separates regions of different phase velocities of the solitary waves. This difference is mostly due to different density structure of a water column. The density ρ_1 at the top of a pycnocline remains the same for both regions and it is equal to $\rho_1 \approx 1005.65$ kg m^{-3}. On the other hand, the bottom layer density for the west slope of the Słupsk Sill is equal $\rho_2 \approx 1013-1014$ kg m^{-3} while for the east slope of the Słupsk Furrow it is equal only $\rho_2 \approx 1008-1010$ kg m^{-3}. It means that dense bottom water from the Bornholm Basin is not able to overflow through the Słupsk Sill, being blocked at the west slope of the Słupsk Sill.

Eq. (38) indicates that internal wave height is proportional to the phase velocity as $H(x) \approx C_p^{-4/3}(x)$. Therefore for the same value of the density parameter $(\rho_2 - \rho_1)/(\rho_1 + \rho_2)$, smaller phase velocity corresponds to a higher wave. That is illustrated in Fig. 10 by comparison of two groups of data for the west slope of the Słupsk Sill and the east slope of the Słupsk Furrow. The following reference values of the wave heights for both regions have been used for calculations: $H(x_0 = 172) = 1$ m and $H(x_0 = 244) = 1$ m.

Another factor which can influence the phase speed and wave height is the thickness of a pycnocline. As it is shown in Fig. 11, thickness of the pycnoclines is changed linearly with water depth h in both regions under consideration. On the west slope of the Słupsk Sill, the thickness is bigger than on the east slope of the Słupsk Furrow. It should be noted that pycnocline thickness $(h_2 - h_1)$ is located in a denominator of fraction in the formula for Väisälä-Brent frequency $N_0(x)$ (see Eq. (47)). Therefore, the smaller pycnocline thickness should

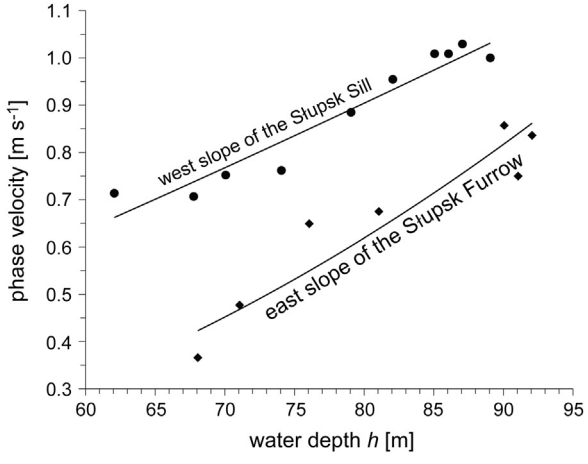

Figure 8 Comparison of phase velocity as a function of water depth for the west slope of the Słupsk Sill and the east slope of the Słupsk Furrow. Solid curves denote the best fitting of simulation data.

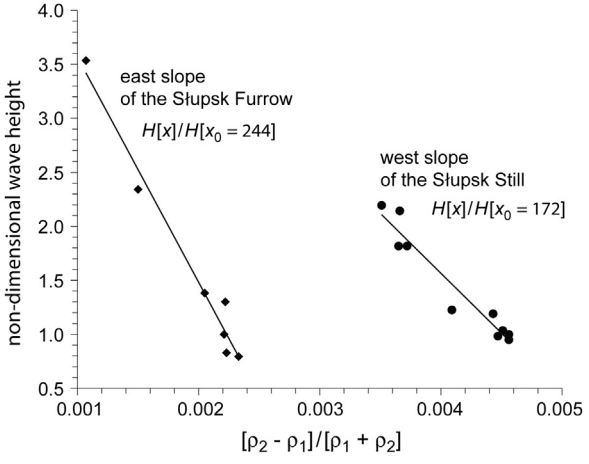

Figure 10 Non-dimensional wave height as a function of density parameter for the west slope of the Słupsk Sill and the east slope of Słupsk Furrow. Solid curves denote the best fitting of simulation data.

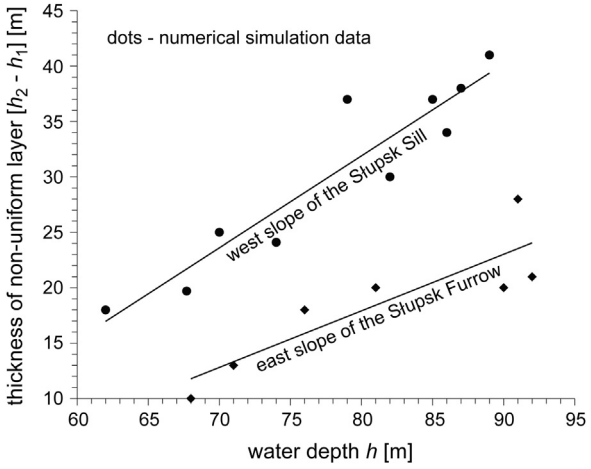

Figure 11 Thickness of non-uniform layer as a function of water depth. Solid curves denote the best fitting of simulation data.

give higher frequency $N_0(x)$ and *vice versa*. Despite this fact, the influence of the density ratio (ρ_2/ρ_1) on frequency $N_0(x)$ is much stronger resulting finally in the higher value of the Väisälä-Brunt frequency on the west slope of the Słupsk Sill.

Let us now consider a short cnoidal wave (T = 10 min) propagating on the west slope of the Słupsk Sill. In Fig. 12, the relationship of wave height and phase speed on the water depth is shown. Wave height of the short cnoidal wave increases much slower than the solitary wave height (see Fig. 3 for comparison). However, phase speed behaves in a similar way, being independent on the shape of an internal wave.

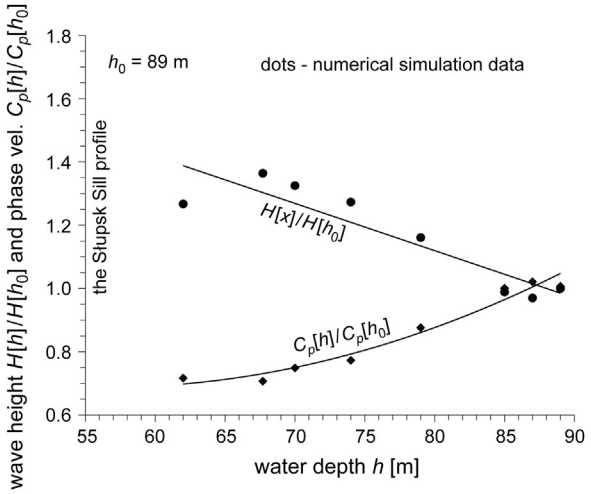

Figure 12 Internal wave height and phase velocity as a function of water depth for short internal wave. Solid curves denote the best fitting of simulation data.

3.3. Wave motion with energy dissipation

3.3.1. Influence of bottom friction

In the previous section, propagation of the internal waves over varying water depth was discussed under assumption that the energy dissipation is absent. When waves are non breaking and the energy loss by percolation is neglected, the only dissipation mechanism is the bottom friction, i.e. $D(x) = D_{fr}$. Then, the energy flux becomes:

$$\frac{d\overline{F_E(x)}}{dx} + D(x) = 0, \tag{54}$$

in which the average work done by friction stress for periodic wave per unit area is (Massel, 2012):

$$D = \overline{\tau u_b} = \frac{1}{T}\int_0^T \overline{\rho} f u_b^2 |u_b|\, dt, \tag{55}$$

where f_r is the friction factor ($f_r \approx 0.05$) and u_b is the bottom velocity due to internal waves:

$$u_b(x,t) = -C_p(x)(x)\eta(x,t)\left(\frac{d\Phi(x,z)}{dz}\right)_{z=-h}. \tag{56}$$

First let us apply above relationships for the cnoidal waves of arbitrary elliptic parameter m. Thus, the dissipation term D_{fr} becomes:

$$D(x) = -P_2(x)H^3(x), \tag{57}$$

in which:

$$P_2(x) = \overline{\rho}(-h) f_r C_p^3(x)\left(\frac{d\Phi(x,z)}{dz}\right)_{z=-h}^3 \sum_{i=1}^{4} B_i(x), \tag{58}$$

and

$$B_1(x) = \left[\frac{1}{m}\left(1-\frac{\mathbf{E}}{\mathbf{K}}-m\right)\right]^3, \tag{59}$$

$$B_2(x) = \frac{-3}{m^3}\left(1-\frac{\mathbf{E}}{\mathbf{K}}-m\right)^3, \tag{60}$$

$$B_3(x) = \frac{1}{m^3}\left(1-\frac{\mathbf{E}}{\mathbf{K}}-m\right) \times \left\{m(m-1)-2(2m-1)\left[1-\frac{\mathbf{E}}{\mathbf{K}}-m\right]\right\}, \tag{61}$$

$$B_4(x) = \frac{1}{5m^3}\left\{\frac{4}{3}(2m-1)\left[m(1-m)-2(2m-1)\left(1-\frac{\mathbf{E}}{\mathbf{K}}-m\right)\right] -3m(1-m)\left[1-\frac{\mathbf{E}}{\mathbf{K}}-m\right]\right\}. \tag{62}$$

Substituting Eq. (57) into Eq. (27) provides the governing equation for wave amplitude $H(x)$ in a form of the Bernoulli equation:

$$\frac{dH(x)}{dx} + \frac{1}{2}\frac{\frac{dP_1(x)}{dx}}{P_1(x)}H(x) + \frac{1}{2}\frac{P_2(x)}{P_1(x)}H^2(x) = 0, \tag{63}$$

which has the following solution:

$$H(x) = \left(\frac{P_1(x_0)}{P_1(x)}\right)^{1/2} G^{-1}(x, x_0) H(x_0), \tag{64}$$

where:

$$G(x) = 1 + \frac{1}{2}\overline{\rho}(-h) f_r H \times (x_0) P_1^{1/2}(x_0) \int_{x_0}^{x} P_1^{-3/2}(x) \hat{P}_2(x)\, dx \tag{65}$$

and

$$\hat{P}_2(x) = C_p^3(x) \left(\frac{d\Phi(x,z)}{dz}\right)^3_{z=-h} \sum_{i=1}^{4} B_i(x). \tag{66}$$

For the solitary waves, if $m = 1$, the energy flux, the dissipation term and the wave height become:

$$\overline{F_E(x)} = P_1(x) H^{3/2}(x) = \frac{4\sqrt{3}}{3} \times C_p^2(x) \Pi(x) \left(\frac{\hat{\beta}(x)}{\hat{\alpha}(x)}\right)^{1/2} H^{3/2}, \tag{67}$$

$$D_{fr} = P_2(x) H^{5/2}(x) = \frac{16\sqrt{3}}{15} C_p^2(x) \overline{\rho}(-h) f_r \times \left(\frac{d\Phi(x,z)}{dz}\right)_{z=-h} \left(\frac{\hat{\beta}(x)}{\hat{\alpha}(x)}\right)^{1/2} H^{5/2}, \tag{68}$$

$$H(x) = \left(\frac{P_1(x_0)}{P_1(x)}\right)^{2/3} G^{-1}(x, x_0) H(x_0), \tag{69}$$

where:

$$G(x, x_0) = 1 + \frac{2}{3}\overline{\rho}(-h) f_r H(x_0) P_1^{2/3}(x_0) \times \int_{x_0}^{x} P_1^{-5/3}(x) \hat{P}_2(x)\, dx \tag{70}$$

and

$$\hat{P}_2(x) = \frac{16\sqrt{3}}{15} C_p^2(x) \left(\frac{d\Phi(x,z)}{dz}\right)^3_{z=-h} \left(\frac{\hat{\beta}(x)}{\hat{\alpha}(x)}\right)^{1/2}. \tag{71}$$

We illustrate an influence of the bottom friction on the propagation of solitary waves on west slope of the Słupsk Sill for the initial wave height $H = 3$ m and friction factor $f_r = 0.05$. In Fig. 13, the ratio of the wave height $H_{fr}(x)/H(x)$ is shown, where H_{fr} is the wave height including the bottom friction and $H(x)$ is wave height without dissipation. Reduction of wave height due to bottom friction is very small, being less than 1.5% for water depth decreasing along the slope from 89 m till 62 m.

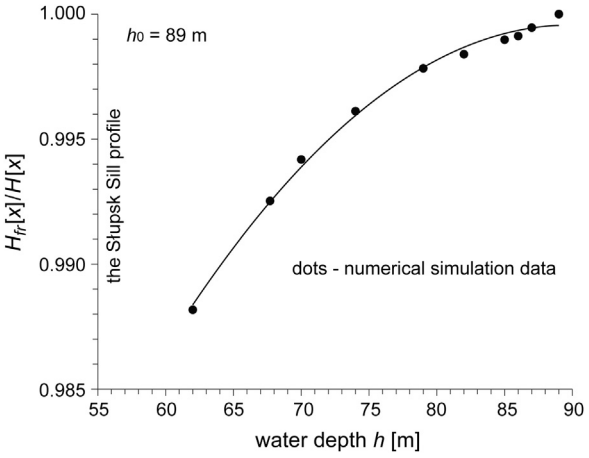

Figure 13 Influence of bottom friction on dynamics of solitary wave height. Solid curves denote the best fitting of simulation data.

3.3.2. Shearing instability and mixing

Except the bottom friction, internal wave energy is decreasing by radial spreading and mixing in the water column where the passing wave generates high shear. The energy loss due to shear-induced mixing may be enhanced for shoaling internal waves on shelf. Following Bogucki and Garrett (1993), we examine an influence of the solitary wave height on attenuation of the Richardson number *Ri*. Let the basic state consist steady, shearing flow with dominated horizontal flow. The governing equation for such flow is the Taylor–Goldstein equation for the vertical structure of a perturbation in a stratified flow. The question is now, what is the critical velocity shear below which the flow is stable and above which mixing occurs. This limiting velocity can be determined from the Richardson number (Kundu et al., 2016):

$$Ri(x,z) = \frac{N^2(x)}{\left(\frac{du(x)}{dz}\right)^2}. \tag{72}$$

When $Ri(x, z) > 1/4$ holds everywhere in the domain, the stratified shear flow is stable. On the other hand, criterion $Ri(x, z) < 1/4$ is a necessary but not sufficient condition for instability. In our case for the Richardson number we obtain:

$$Ri(x,z) = \frac{N^2(x)}{\left(C_p(x)(x)\eta(x)\frac{d^2\Phi(x,z)}{dz^2}\right)^2}, \tag{73}$$

where function $\Phi(x, z)$ is given in Eq. (48). For the three-layer vertical density distribution, Eq. (73) is applicable only in the non-uniform layer when $-h_2 < z - h_1$. In the upper uniform layer $(-h_1 \le z \le 0)$ and in the lower uniform layer $(-h \le z \le -h_2)$, the second derivative of function $\Phi(x, z)$ is equal to zero and the Richardson number $Ri(x, z)$ cannot be determined.

Fig. 14 shows distribution of the Richardson number in the non-uniform layer for Station 199 at west slope of the Słupsk Sill when internal wave height ~26 m. The area where the Richardson number $Ri(x, z) < 1/4$ is concentrated under the wave crest and below the upper level of non-uniform layer. This area is rather small, even for very big wave height. The minimum value of the Richardson number drops to about 0.17.

Bogucki and Garrett (1993) argued that for a two-layer system separated by a thin interface with a finite density gradient, the Richardson number in the interface falls below 1/4 if the internal wave height exceeds $2[(h_2 - h_1)\, h_1]^{1/2}$. For such wave height a two-layer system generates mixing by

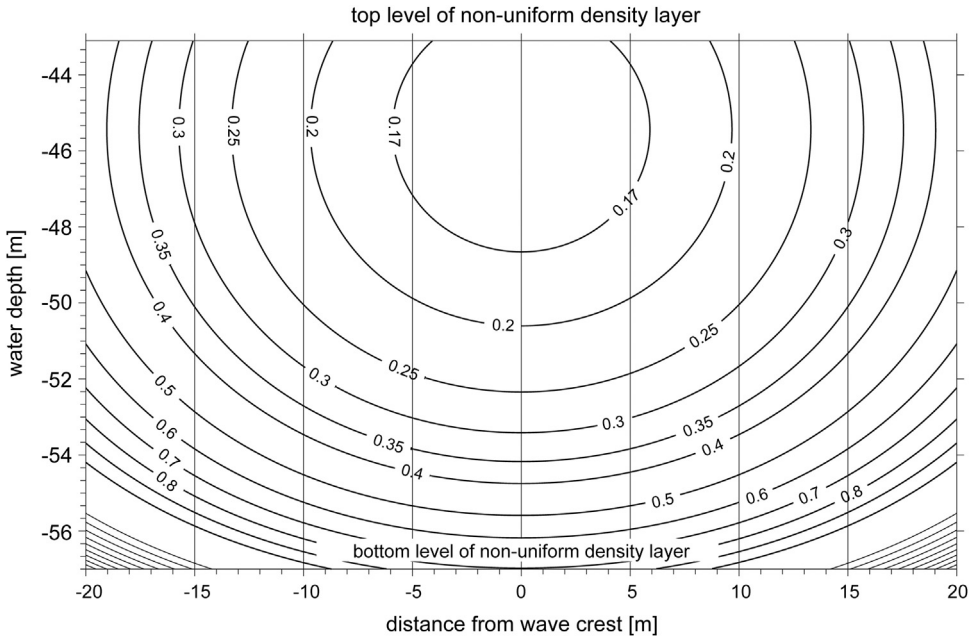

Figure 14 Area of possible shearing instability at the Station 199.

shear instability, and the interface is widening due to passing of internal wave. Bogucki and Garrett (1993), using the concept of interface widening developed a model describing internal wave dissipation and wave height attenuation. However, this model is not applicable as the interface thickness $(h_2 - h_1)$ in our case is not small.

3.3.3. Wave breaking

Numerical calculations by Vlasenko and Hutter (2002) showed that the kinematic instability is responsible for mechanism of strong wave breaking rather than a shearing instability, discussed above. They considered a two-layer system with a vertical fluid stratification. Amplitudes of waves and the bottom parameters were chosen to be close to those observed in the Andaman and Sulu Seas. A proposed breaking criterion for the internal solitary waves for sea bottom slope in the range $0.52^\circ < \beta < 21.8^\circ$ is:

$$\frac{H}{h_b - h_m} \geq \frac{0.8^\circ}{\beta} + 0.4, \tag{74}$$

where H is the maximum displacement at the centre of wave, β is the bottom slope, h_b is the water depth at point of wave breaking and h_m is the depth of an undisturbed position of the interface line. If the water depth on the shelf is less than h_b, a solitary wave breaks before it and penetrates into the shallow water zone, otherwise it passes into the shelf without breaking.

Laboratory experiments by Helfrich and Melville (1986) and Helfrich (1992) showed that wave breaking occurs when normalised maximal wave height $H/(h_b - h_m)$ exceeds 0.4 and does not depends on the bottom slope, i.e.:

$$\frac{H}{h_b - h_m} \geq 0.4. \tag{75}$$

Observations of Lien et al. (2014) on the Dougsha slope (about 0.4°) in the northern South China Sea confirmed that convective breaking of the solitary internal waves, with negative displacement, occurs at $H/(h - h_m) \geq 0.4$, in agreement with the Helfrich's laboratory results.

For typical three-layer density structure, discussed above, determination of the wave breaking criteria is more complicated. First, we apply criterion (75) and assume that depth h_m coincides with a level of the maximum eigenfunction $\Phi(x, z)$, defined by the linear boundary value problem (10) at which $d\Phi(x, z)/dz = 0$. At this level, the isopycnal displacement $\zeta(x)$, given in Eq. (3), has the maximum value.

The second breaking criterion follows from assumption that location of the wave breaking is defined at a position where the horizontal velocity u begins to surpass the phase speed $C_p(x)$ at some level z in water column, i.e.:

$$|u(x, z)| > C_p(x). \tag{76}$$

Numerical simulations showed that for the three-layer density structure, the velocity $|u(x, z)|$ reaches a maximum value close to the sea bottom. Therefore, this value was used for comparison with the phase speed. In Fig. 15 a comparison of the limiting wave heights for both breaking criteria is shown for some Stations on the west slope of the Słupsk Sill, starting from deeper water in the Bornholm Basin and going easterly up to the Słupsk Sill. At the deeper section of the slope, up to Station 193, criterion (76) requires much bigger wave height $H(x)$ than criterion (75). For smaller depths (from Section 193 till Section 199), waves break after reaching criterion (76) and before criterion (75) is satisfied. It should be noted that these results are based on the numerical simulation for real bathymetry and experimental density stratification. However, due to lack of the experimental data on the wave height, these conclusions should be taken only as some estimations of the real breaking process.

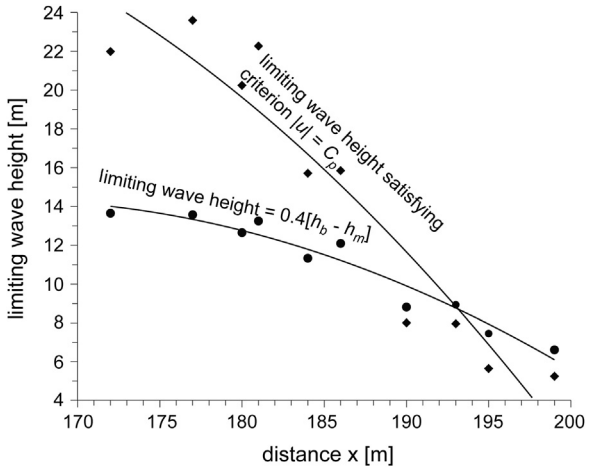

Figure 15 Comparison of two breaking criteria for the west slope of the Słupsk Sill. Solid curves denote the best fitting of simulation data.

4. Conclusions

In this paper, dynamics of the internal cnoidal and solitary waves propagating on horizontally inhomogeneous shallow water is studied. For slowly varying background environment (water depth and density stratification), the theoretical formulae for the wave height and wave shape parameters are derived in an explicit forms, based on the concept of the conservation of energy flux with various energy dissipation terms.

The numerical simulations were applied for the southern Baltic Sea, along the transect from the Bornholm Basin, through the Słupsk Sill and Słupsk Furrow to the Gdańsk Basin. An increase of wave height and decrease of the phase speed in shallowing water depth was illustrated. The bottom friction has only negligible influence on the dynamics of internal waves, while the shearing instability may be important only for very large wave heights. The area of the possible instability, expressed in terms of the Richardson number Ri, is very small and restricted to an area within the non-uniform density layer, close to the upper uniform layer. The kinematic breaking criteria, suggested by Helfrich and Vlasenko and Hutter, have been examined and critical internal wave heights for the three-layer density structure have been determined.

Acknowledgments

This work has been supported by the Programme *Natural and antropogenic variability of the Baltic Sea environment* of the Institute of Oceanology of the Polish Academy of Sciences. I am thankful to the reviewers for their suggestions and comments.

References

Abramowitz, M., Stegun, I.A., 1975. Handbook of Mathematical Functions with Formulas, Graphs, and Mathematical Tables. Dover Publ., New York, 1075 pp.

Bogucki, D., Garrett, Ch., 1993. A simple model for the shear-induced decay of an internal solitary wave. J. Phys. Oceanogr. 23 (8), 1767–1776.

Gill, A.E., 1982. Atmosphere-Ocean Dynamics. Academic Press, New York, 662 pp.

Gradshteyn, I.S., Ryzhik, I.M., 1965. Tables of Integrals, Series and Products. Academic Press, New York, 860 pp.

Grimshaw, R., Guo, Ch., Helfrich, K., Vlasenko, V., 2014. Combined effect of rotation and topography on shoaling oceanic internal solitary waves. J. Phys. Oceanogr. 44 (4), 1116–1132.

Grimshaw, R., Pelinovsky, E.N., Talipova, T., Kurkin, A., 2004. Simulation of the transformation of internal solitary waves on oceanic shelves. J. Phys. Oceanogr. 34 (1), 2774–2791.

Helfrich, K.R., 1992. Internal solitary wave breaking and run-up on a uniform slope. J. Fluid Mech. 243, 133–154.

Helfrich, K.R., Melville, W.K., 1986. On long nonlinear internal waves over slope-shelf topography. J. Fluid Mech. 167, 285–308.

Holloway, P.E., 1994. Observations of internal tide propagation on the Australian North West Shelf. J. Phys. Oceanogr. 24, 1706–1716.

Holloway, P.E., 1996. A numerical model of internal tides with application to the Australian North West Shelf. J. Phys. Oceanogr. 26, 21–37.

Korteweg, D.J., de Vries, G., 1895. On the change of form of long waves advancing in a rectangular canal, and on a new type of stationary waves. Phil. Mag. J. Sci. 39, 422–443.

Krauss, W., 1966. Interne Wellen. Gebruder Borntraeger, Berlin, 248 pp.

Kundu, P.K., Cohen, I.M., Dowling, D.R., 2016. Fluids Mechanics, sixth edition. Elsevier, Amsterdam, 921 pp.

Kurkina, O., Talipova, T.G., Pelinovsky, E.N., Soomere, T., 2011. Mapping the internal wave field in the Baltic Sea in the context of sediment transport in shallow water. J. Coast. Res. 64, 2042–2047.

Lien, R.C., Henyey, F., Ma, B., 2014. Large-amplitude internal solitary waves observed in the Northern South China Sea: properties and energetics. J. Phys. Oceanogr. 44 (4), 1095–1115.

Massel, S.R., 1989. Hydrodynamics of Coastal Zones. Elsevier, Amsterdam, 336 pp.

Massel, S.R., 2012. Tsunami in coastal zone due to meteorite impact. Coastal Eng. 66, 40–49.

Massel, S.R., 2015. Internal Gravity Waves in the Shallow Seas. GeoPlanet: Earth and Planetary Sciences. Springer Int. Publ, Switzerland, 163 pp.

Miles, J.W., 1981. The Korteweg-de Vries equation: a historic essay. J. Fluid Mech. 106, 131–147.

Pelinovsky, E.N., Shavratsky, S.Kh., 1976. Propagation of nonlinear internal waves in an inhomogeneous ocean. Izv. Atmos. Ocean. Phys. 12 (1), 41–44.

Pelinovsky, E.N., Stepanyants, Yu., Talipova, T.G., 1994. Modelling of the propagation of nonlinear internal waves horizontally inhomogeneous ocean. Izv. Atmos. Ocean. Phys. 30 (1), 79–85.

Piechura, J., Beszczyńska-Möller, A., 2004. Inflow waters in the deep regions of the southern Baltic Sea — transport and transformations. Oceanologia 46 (1), 113–141.

Talipova, T.G., Pelinovsky, E.N., Kouts, T., 1998. Kinematic characteristics of an internal wave field in the Gotland Deep in the Baltic Sea. Oceanology, Translated from Okeanologiya 38, 33–42.

Vlasenko, V., Hutter, K., 2002. Numerical experiments on the breaking of solitary internal waves over a slope-shelf topography. J. Phys. Oceanogr. 32 (6), 1779–1793.

Whitham, G.B., 1974. Linear and Nonlinear Waves. Wiley, New York, 636 pp.